International Journal of GEOMATE, Jan., 2018 Vol.14, Issue 41, pp.77-85
Geotec., Const. Mat. & Env., DOI: https://doi.org/10.21660/2018.41.19423
ISSN: 2186-2982 (Print), 2186-2990 (Online), Japan

UNIAXIAL COMPRESSIVE STRESS-STRAIN BEHAVIOR OF SELF-COMPACTING CONCRETE WITH HIGH-VOLUME FLY ASH

*Stefanus A Kristiawan[1], Agus Setiya Budi[2], and Andreas Nur Hadi[2]

[1]SMARTCrete Research Group, Civil Engineering Department, Engineering Faculty, Universitas Sebelas Maret, Indonesia; [2]Civil Engineering Department, Engineering Faculty, Universitas Sebelas Maret, Indonesia

*Corresponding Author, Received: 31 Aug. 2017, Revised: 22 Sept. 2017, Accepted: 30 Oct. 2017

ABSTRACT: Complete stress-strain behavior is a fundamental characteristic of concrete from which principle parameters in the analysis and design of structural concrete elements are developed. It is recognized that the stress-strain behavior of concrete under uniaxial compressive loading is influenced by the concrete constituents. A special type of concrete, i.e. self-compacting concrete (SCC) incorporating high-volume fly ash, has different constituents to that of conventional concrete. For this reason, characterization of the complete stress-strain behavior of this type of concrete is necessary for reliable analysis, design, and utilization of this concrete as a structural element. This research aims to investigate the complete stress-strain behavior of SCC, incorporating a variety of high-volume fly ash (50–70% by weight of total binder) under uniaxial compressive loading. The compression tests were carried out on cylinder specimens of 75×150 mm, where the deformation was controlled at a rate of 1.5mm/min. The results show that at a stress below 60% of peak value, there is a linear relationship of stress and strain. In this state, both global and local longitudinal deformation is quite similar. However, above this stress level, a nonlinearity of the stress and strain relationship exists and local deformation at the fracture zone is higher than global deformation. Various stress-strain models have been used to capture the complete stress-strain diagram of the investigated concrete, using key parameters of the diagram as inputs. Most of the models give a better prediction in the ascending part compared to that of the descending branch. In general, Samani and Attard's model gives the lowest coefficient of variation of error than other models.

Keywords: Deformation, High volume fly ash, Self-compacting concrete, Stress-strain model

1. INTRODUCTION

Sustainability is a major issue affecting the activities of concrete industries around the globe, because concrete is not a sustainable construction material for a variety of reasons. The main concern with using of concrete is that it requires a significant quantity of cement, the production of which generates CO_2 emissions, which contribute to the greenhouse gas effect [1]. Attempts have been made to seek alternative construction materials with a smaller environmental impact, by reducing the amount of cement. One of these is the use of high-volume fly ash to partially replace cement content in the production of construction materials [1-3]. In previous research, a special type of concrete i.e. self-compacting concrete (SCC) was produced by incorporating high-volume fly ash to substitute the cement content in the range of 50–70% by weight. The influences of high-volume fly ash on short-term and long-term properties are noted [4-9]. To support the utilization of this type of concrete as a structural element, a reliable stress-strain relationship must be determined carefully. Complete stress-strain behavior of concrete is a very important characteristic from which fundamental parameters in the analysis and design of structural concrete elements can be developed [10,11].

It has been shown by previous researchers [12-15] that the complete stress-strain behavior of concrete under uniaxial compressive loading is affected by the type of concrete being investigated. Belen et al. [13] used recycled saturated coarse aggregate to substitute normal coarse aggregate at various percentages in the production of concrete. They confirmed that due to the low elastic modulus of recycled coarse aggregate compared to normal aggregate, the recycled aggregate concrete exhibited greater strains under similar stresses compared to the normal concrete. The effect of aggregate type on the stress-strain behavior was also suggested by Da et al [14]. The descending part of the complete stress-strain curve showed a sudden drop (no softening behavior) for concrete with corals as the substitute for aggregates. The no softening behavior of the descending part of the stress-strain curve was similarly observed in concrete with different types of cementitious material; i.e. Geopolymer Concrete [15].

The amount of coarse aggregates in SCC is lower compared to conventional concrete. On the other hand, the amount of fine particles, including cement, is higher in SCC [16]. This proportion of ingredients in SCC could be expected to give a different behavior to the stress-strain relationship.

An inclusion of high-volume fly ash to substitute a large quantity of cement in SCC may give further distinction to the behavior. The difference in the stress-strain behavior due to the difference in concrete composition could be explained by various fracture mechanisms at the meso- and macro-level, as suggested by Van Mier [17]. Relatively higher and lower amounts of fine and coarse particles in SCC, compared to normal concrete, will affect the arrangement of particles of hardened concrete, which influences the stress distributions and concentrations via particle contacts, eventually triggering microcracking in the weak bonding between aggregates and cementitious material. The microcracking is accountable for the nonlinear stress-strain behavior in the prepeak region. Some of the microcracks propagate and develop into stabilized cracks in a localized fracture zone, which affects the softening response in the postpeak region [17-19].

Several models have been suggested to represent the complete stress-strain behavior of concrete under uniaxial loading [10, 20-27]. Three of these were selected for the purpose of assessing the suitability of the models to capture the stress-strain behavior of SCC incorporating high-volume fly ash. The first model is that proposed by Carreira and Chu [20]. The relationship of stress (f_c) and strain (ε) by this model is expressed by the following equations:

$$\frac{f_c}{f'_c} = \frac{\beta\left[\frac{\varepsilon}{\varepsilon'_c}\right]}{\beta - 1 + \left[\frac{\varepsilon}{\varepsilon'_c}\right]^{\beta}} \tag{1}$$

and

$$\beta = \frac{1}{1 - \frac{f'_c}{E_{it}}} \tag{2}$$

for $\beta \geq 1$ and $\varepsilon \leq \varepsilon_u$

where f'_c, ε'_c, ε_u and E_{it} are peak stress, peak strain, ultimate strain and initial elastic modulus of concrete, respectively. These parameters can be determined from the compression test data of the stress-strain diagram, in which the deformation rate is controlled. Carreira and Chu's model has been used to fit various experimental data, using a minimization of the square of the error technique. The experimental data of stress-strain diagrams for the above curve fitting vary in terms of strength (8.96 MPa to 139 MPa), specimen size and shape, age of specimen, and type of concrete (normal weight and lightweight concrete). Close agreement between the fitted curves and experimental data suggests that the model could be used to represent the complete stress-strain relationship in compression for a wide range of concrete characteristics and testing conditions.

The second selected stress-strain model is that of Samani and Attard [21]. The model was developed to predict complete stress-strain behavior of concrete, both under uniaxial and triaxial (confined) compressive loading. They proposed a separate equation to represent the ascending and descending parts of the stress-strain diagram. The stress (f_c) and strain (ε) relationship for the ascending branch (where $\varepsilon \leq \varepsilon_o$) is given by the following equations:

$$\frac{f_c}{f_o} = \frac{A.\frac{\varepsilon}{\varepsilon_o} + B.\left(\frac{\varepsilon}{\varepsilon_o}\right)^2}{1 + (A-2)\frac{\varepsilon}{\varepsilon_o} + (B+1)\left(\frac{\varepsilon}{\varepsilon_o}\right)^2} \tag{3}$$

$$A = \frac{E_c\,\varepsilon_o}{f_o}; \text{ and } B = \frac{(A-1)^2}{0{,}55} - 1 \tag{4}$$

where the secant elastic modulus (E_c), which is measured at a stress level of $0.45f'_c$, is assumed to be similar to the initial elastic modulus (E_{it}). In the case of uniaxial loading, the peak stress (f_o) and strain (ε_o) will be equal to f'_c and ε'_c, respectively. For the descending branch ($\varepsilon \geq \varepsilon_o$), two equations are proposed to calculate postpeak softening (Eq. 5) and the inflection branch (Eq. 6):

$$\frac{f_c}{f_o} = \frac{f_{res}}{f_o} + \left[1 - \frac{f_{res}}{f_o}\right]\left[\frac{f_{ic}}{f'_c}\right]^{\left[\frac{\varepsilon - \varepsilon_o}{\varepsilon_i - \varepsilon_o}\right]} \tag{5}$$

$$\frac{f_i}{f_o} = \frac{f_{res}}{f_o} + \left[1 - \frac{f_{res}}{f_o}\right]\left[\frac{f_{ic}}{f'_c}\right] \tag{6}$$

where f_{res} is residual stress, f_i and ε_i is stress and strain after inflection point (f_{ic}). The uniaxial inflection point (f_{ic}) is defined by Eq. 7:

$$\frac{f_{ic}}{f'_c} = 1.41 - 0.17\ln(f'_c) \tag{7}$$

for $f'_c \geq 20$ MPa

The last selected model is that of *fib* Model Code 2010 [10], as given in Eq. 8 for $\varepsilon \leq \varepsilon_{max}$.

$$\frac{f_c}{f'_c} = \left\{\frac{\left[\frac{E_{it}}{E_c}\right]\left[\frac{\varepsilon}{\varepsilon'_c}\right] - \left[\frac{\varepsilon}{\varepsilon'_c}\right]^2}{1 + \left[\frac{E_{it}}{E_c} - 2\right]\left[\frac{\varepsilon}{\varepsilon'_c}\right]}\right\} \tag{8}$$

ε_{max} is the concrete maximum strain corresponding to a strain at $0.5f'_c$ in the postpeak region. E_c is the secant elastic modulus at peak stress. For $\varepsilon \geq \varepsilon_{max}$, Eq. 9 may be used:

$$\frac{f_c}{f'_c} = \frac{1}{\left[\frac{1}{(\varepsilon_{max}/\varepsilon'_c)}\varphi - \frac{2}{(\varepsilon_{max})/\varepsilon'_c)^2}\right]\left(\frac{\varepsilon}{\varepsilon'_c}\right)^2 + \left[\frac{4}{\left(\frac{\varepsilon_{max}}{\varepsilon'_c}\right)} - \varphi\right]\frac{\varepsilon}{\varepsilon'_c}} \tag{9}$$

where

$$\varphi = \frac{4\left[\left(\frac{\varepsilon_{max}}{\varepsilon'_c}\right)^2\left(\frac{E_{it}}{E_c} - 2\right) + 2\left(\frac{\varepsilon_{max}}{\varepsilon'_c}\right) - \frac{E_{it}}{E_c}\right]}{\left[\left(\frac{\varepsilon_{max}}{\varepsilon'_c}\right)\left(\frac{E_{it}}{E_c} - 2\right) + 1\right]^2} \tag{10}$$

This research aims to characterize the complete stress-strain behavior of SCC incorporating high-volume fly ash, and to evaluate the suitability of the above models for capturing the stress-strain behavior of the mentioned concrete. A coefficient of variation (COV) of error [5] will be used to quantify the conformity between the values estimated by the models and the experimental data of stress-strain diagrams. The results could be useful in the development of the analysis and design of structural elements utilizing SCC with high-volume fly ash.

2. MATERIALS AND TESTING

2.1 Materials and Composition of SCC

All materials for producing the specimens were tested following the respected standards. The specific gravity and gradation of the coarse (CA) and fine aggregates (FA) were determined according to ASTM C128 and ASTM C136, respectively. The measured apparent specific gravity was 2.73 and 2.70 for coarse and fine aggregates, respectively, and the corresponding fineness modulus was 5.69 and 2.98. The cement was a type of Portland pozzolanic cement conforming to ASTM C595, whereas fly ash was supplied from the Cilacap Power Plant. The chemical composition of fly ash is given in Table 1. A polycarboxylate-based superplasticizer (Sp) was used to realize the flowability of fresh concrete.

The composition of SCC was formulated following the principles set out by Okamura and Ozawa [16]. The final composition of SCC incorporating various fly ash content (50–70% by weight of total binder) is presented in Table 2. The flowability of the SCCs is given in Table 3.

2.2 Specimens and Testing

Three cylinder specimens of 75×150 mm were cast for each mix proportion. The specimens were cured under wet burlap for 21 days, and then stored in the laboratory environment for 7 days. The specimens were finally tested under uniaxial compression test at 28 days of age.

The compression loading was carried out using a Universal Testing Machine (UTM), where the deformation was controlled at a rate of 1.5 mm/min. It is worth noting that there was no intention to reduce the friction between the loading platens and the specimens during testing. The deformation of the specimens was measured using two instruments. The first was the longitudinal displacement of the loading platen of the UTM, sensed by the embedded transducer in the machine. This deformation represented the global longitudinal deformation of the specimen at a gauge length of 150 mm. The second longitudinal deformation was a local deformation at the midheight of the specimen, with a gauge length of 60 mm. This second deformation was sensed using a strain gauge which was attached on the surface of the specimen. In addition to those of longitudinal deformations, a strain gauge of 60 mm gauge length was also attached radially at the midheight of the specimen (Fig. 1). The radial strain gauge could be used to determine the lateral deformation. The fracture mode of the specimens was captured by camera (Fig. 2)

Table 1. Chemical composition of fly ash

SiO_2	Al_2O_3	Fe_2O_3	TiO_2	CaO	MgO	K_2O	Na_2O	P_2O_5	SO_3	MnO_2
45.27	20.07	10.59	0.82	13.32	2.83	1.59	0.98	0.41	1	0.07

Table 2. Composition of SCC

Specimen ID	Cement (kg/m^3)	Fly ash (kg/m^3)	CA (kg/m^3)	FA (kg/m^3)	Water (lt/m^3)	Sp (lt/m^3)
SCC-50%	384.30	384.3	709.8	595.35	231	7.686
SCC-55%	345.87	422.73	709.8	595.35	231	7.686
SCC-60%	307.44	461.16	709.8	595.35	231	7.686
SCC-65%	269.01	499.59	709.8	595.35	231	7.686
SCC-70%	230.58	538.02	709.8	595.35	231	7.686

Table 3. Flowability of SCC

Flow parameter	SCC-50%	SCC-55%	SCC-60%	SCC-65%	SCC-70%
diameter (mm)	750	745	755	760	765
t500 (sec)	3.61	3.60	3.47	3.31	3.25
velocity (mm/sec)	138.5	138.9	144.1	151.1	153.8

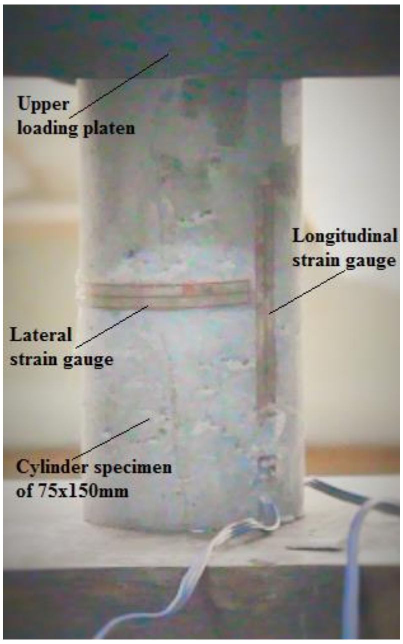

Fig.1. Longitudinal and lateral strain gauge attached on surface of specimen

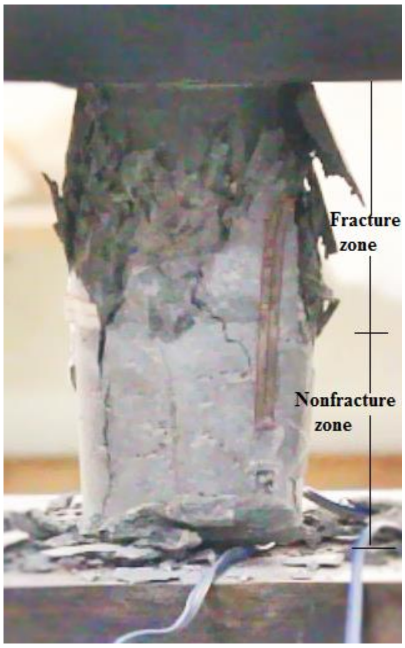

Fig. 2. Fracture and nonfracture zone of cylinder specimen

3. RESULTS AND DISCUSSIONS

3.1 Longitudinal Strain

An example of the measured stresses up to failure, and their corresponding longitudinal strains on a single specimen under uniaxial loading, is presented in Fig. 3. A complete stress-strain diagram was determined using data of global longitudinal deformations, measured by the embedded transducer of the UTM. The strain gauge could only measure data of strains up to about 80% of the peak value. It also confirmed that initially the strains measured by both the strain gauge and the embedded transducer of the UTM were approximately equal in magnitude. However, the longitudinal strains measured by strain gauge started to deviate from those measured by UTM at about 60% of the peak value. This behavior could be related to the development of a fracture zone on the specimen. Under low stress level, no microcracks appeared in the concrete specimen, and the specimen behaved as a linear elastic material. The strains measured by the two sensors (strain gauge and tranduscer of UTM) could be expected to give similar magnitude of strains in this state. When the stress increased, microcracks began to appear and affected the deformation of the specimen. The local longitudinal deformation measured on the microcracking zone was greater than that observed at a global level. Considering the friction provided by the loading platens, and the ratio of the height to the diameter (h/d=2) of the specimen [19], it could be expected that the microcracks would start to develop at around the midheight of the specimen. Consequently, the strains measured by the strain gauge were more sensitive than those measured by the UTM transducer. In fact, the global longitudinal deformation measured by the transducer consisted of deformations on both the fracture zone and nonfracture zone. Hence, the magnitude of the global longitudinal deformation may be viewed as an average value of the longitudinal deformation in the fracture and nonfracture zones. The fracture zone of the specimen confirmed the above circumstances (see Fig. 2).

3.2 Radial or Lateral Strain

The stress-radial/lateral strain relationship on a single specimen is shown in Fig. 4. The measured strain stopped when the stress reached 21.8 MPa; i.e. about 80% of the peak value. The radial/lateral strains have a similar pattern to that of longitudinal strains measured by strain gauge. The stress-strain relationship was initially a linear elastic up to a stress of about 60% of the peak value, after which, the curve started to bend over, indicating the initiation of microcracks and their subsequent propagation. It is recognized that due to the friction stresses instigated by loading platens, the specimen would deform radially under compressive loading, with the maximum expansion occurring somewhere within the fracture zone [Fig. 2]. When microcracks start to appear and propagate under increasing stress, the radial expansion is accelerated. This gives an increased rate of radial strain with a constant of

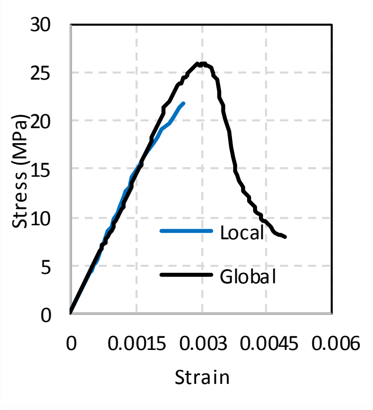

Fig. 3. Stress and its corresponding local and global longitudinal strains

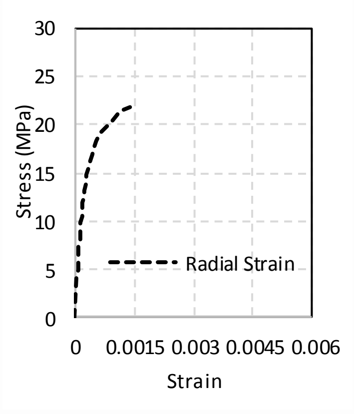

Fig. 4. Stress and radial strain

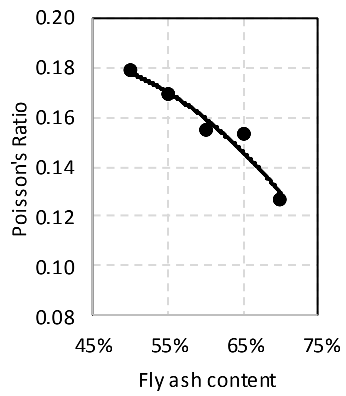

Fig. 5. Effect of fly ash on Poisson's ratio

Table 4. Key parameters of stress-strain diagram

Specimen	f'_c (MPa)	ε'_c	ε_{max}	f_{ic} (MPa) *	f_{ic} (MPa) **	f_{res} MPa
SCC-50%	25.66	0.00278	0.00387	22.02	10.36	4.74
SCC-55%	24.60	0.00275	0.00365	21.29	9.43	4.48
SCC-60%	23.40	0.00269	0.00380	20.45	10.10	3.43
SCC-65%	22.38	0.00246	0.00356	19.80	9.27	3.06
SCC-70%	19.89	0.00252	0.00370	17.90	8.70	3.07

** theoretical; **experimental;* f'_c*=peak stress;* ε'_c*=peak strain;* ε_{max}*=maximum strain;* f_{ic}*=inflextion point;* f_{res}*=residual stress*

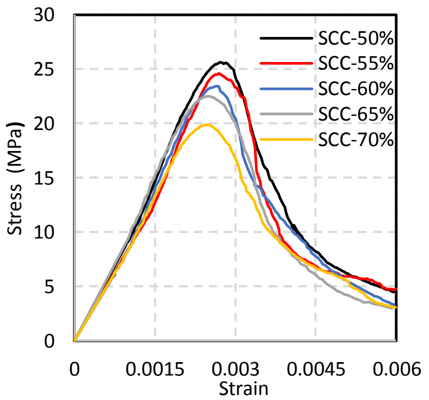

Fig. 6 Complete stress-strain behavior of SCC with various fly ash content

increment of stress. The strain gauge was disrupted when the microcracks turned into larger cracks, and so it was not able to measure further strain. This coincided with a stress at about 80% the peak value.

The ratio of the radial/lateral strain to the longitudinal strain, or the Poisson's ratio of all the specimens, is presented in Fig. 5. The ratio is calculated on the basis of measured strains at a stress equal to 40% of the peak value. The Poisson's ratio of the SCC incorporating various high-volume fly ash is in the range of 0.114–0.179, which is within the range of common concrete (0.1–0.2). Figure 5 shows that increasing the amount of the fly ash tends to decrease the Poisson's ratio. This may be related to the more ductile behavior of the SCC incorporating more fly ash, which will be shown in the next section.

3.3 Complete Stress-Strain Curve

As mentioned previously, the complete stress-strain curve can only be obtained from the measurement of global axial strain using the embedded UTM transducer. Figure 6 shows the complete stress-strain curves of SCC at a variety of fly ash replacement levels. All curves have similar behavior. At the ascending branch, the curve initially shows a linear stress-strain relationship, and then the curve is bent over until reaching its corresponding peak stress. At the descending branch, right after the peak value, a sudden drop of stress is observed at a small increment of strain. However, at about 40% of the peak stress, an inflection point is noticed in the descending branch. The inflection points extracted from the stress-strain diagrams are lower compared to those calculated using Eq. (7), as given in Table 4. After the inflection point, the stress is reduced at a decelerating rate, with an increment of strain. A residual stress is observed at the end of each curve.

Key parameters can be determined from the complete stress-strain curves. These include peak stress, peak strain, maximum strain, inflection point, and residual stress. Table 4 summarizes these key parameters. A higher peak stress is observed in SCC containing less fly ash. This behavior may be explained by the fact that a lower level of fly ash replacement means there is a higher amount of cement in the mix. Consequently, more hydration products to bind the solid constituents are expected in SCC with lower fly ash replacement. Meanwhile, at 28 days of age the pozzolanic reaction of fly ash may not be as influential as at a later age (more than 90 days). In terms of peak strain, the trend is similar to that of the peak stress. A higher level of fly ash replacement gives a lower peak strain. However, the maximum difference in the magnitude of peak strain is not significant; i.e. only 0.4‰. Meanwhile, the maximum strain, defined as the strain at the descending branch corresponding to the stress at 50% of the peak stress, is within a range of 0.00356–0.00387. This maximum stress could be used as a limit in the analysis and design of structural elements, using SCC incorporating high-volume fly ash. The range of values is close to the specified maximum strain in the *fib* Model Code 2010; i.e. 0.0035 for C25 grade of normal weight concrete [10]. Finally, the residual stress of the SCC incorporating high-volume fly ash is in the range of 3.06–4.74 MPa, which represents about 13–18% of its corresponding peak value.

Another useful parameter that could be used to characterize the behavior of concrete is the ductility factor. This parameter could describe the ability of concrete to undergo significant deformation before rupture. There are several methods to quantify the ductility factor. In this research, the ductility factor is quantified as the ratio of the area under complete stress-strain curve to the area under the same curve, but limited to the region below 40% of the peak stress. The area under the stress-strain curve could be viewed as a thoroughness index, where this parameter indicates the ability of the concrete to absorb energy and deform inelastically before rupture. The 40% of peak stress limit is chosen in the computation of the ductility factor since, theoretically, it is considered to be the limit of elasticity. However, this may not always be the case, as shown by the results of this current research, but this theoretical limit is adopted in the quantification of the ductility factor. The ductility factors quantified in this way for all SCCs are presented in Fig.7. There is a tendency for a higher content of fly ash to yield a higher ductility factor. This may be related to the particle packing of the concrete constituents. Fly ash is finer and lower in density than cement. For this reason, a higher replacement of cement with fly ash would cause a greater amount of finer constituents in SCC. Consequently, there is a greater chance of distributing stresses evenly via finer particle contact, and reducing the concentration of stresses around larger interparticles, where this concentration of stresses could create paths of cracking, leading to sudden rupture.

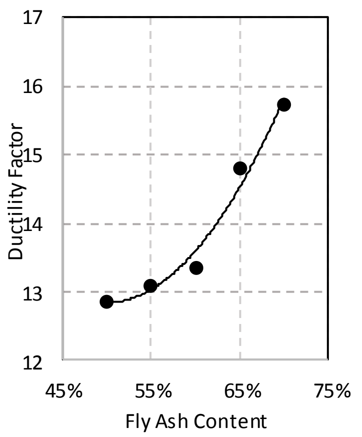

Fig. 7. Ductility factor of SCC for various fly ash content

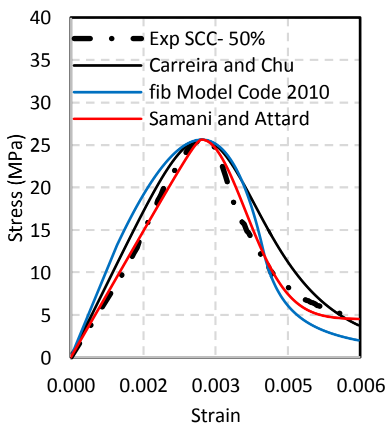

Fig. 8. Experimental stress-strain diagram for SCC-50% and fitted curves by models

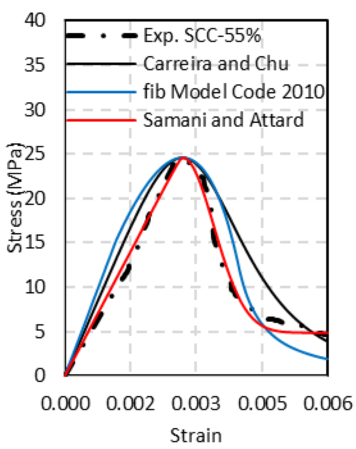

Fig. 9. Experimental stress-strain diagram for SCC-55% and fitted curves by models

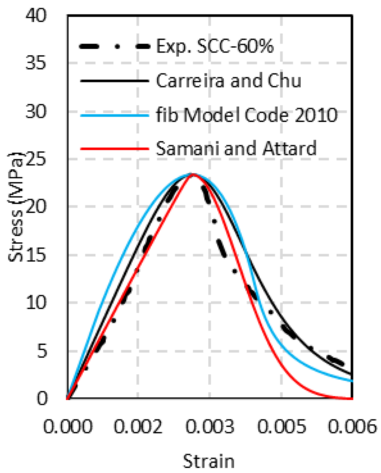

Fig. 10. Experimental stress-strain diagram for SCC-60% and fitted curves by models

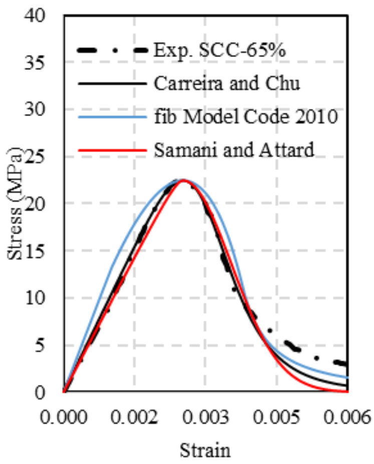

Fig. 11. Experimental stress-strain diagram for SCC-65% and fitted curves by models

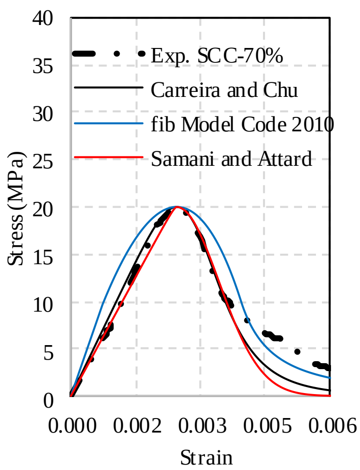

Fig. 12. Experimental stress-strain diagram for SCC-70% and fitted curves by models

Table 5. Coefficient of variation of error for the models

Specimen	Carreira and Chu's model		Samani and Attard's model		*fib* Model Code 2010	
	Ascending	Descending	Ascending	Descending	Ascending	Descending
SCC-50%	9.93%	21.51%	3.75%	9.43%	16.63%	24.36%
SCC-55%	14.63%	29.33%	4.72%	8,32%	19.87%	33.25%
SCC-60%	11.24%	16.72%	5.28%	34.16%	20.31%	33.83%
SCC-65%	2.34%	18.31%	5.10%	25.83%	12.19%	20.36%
SCC-70%	4.93%	33.15%	6.52%	34.76%	17.77%	27.10%
Average	8.61%	23.80%	5.07%	26.05%	17.35%	27.78%

3.4 Complete Stress-Strain Model

Three models were selected to capture the complete stress-strain behavior of SCC incorporating high-volume fly ash. Figures 8–12 illustrate a comparison between the fitted curves of the models and the experimental results of the stress-strain diagrams. A quantification of the prediction models' accuracy was accomplished by the coefficient of variation (COV) of error method. A separate assessment was made for the evaluation of the models; i.e. in the ascending and the descending branch of the curves. The results are presented in Table 5, which shows clearly that all models give better prediction on the ascending part compared to the descending one. The COV computed in the ascending branch is within 2.34–14.63% for Carreira and Chu's model, with an average value of 8.61%. Smaller variations with the experimental data are found in the ascending branch when Samani and Attard's model is used. The COV of Samani and Attard's model is within 3.75–6.52%, with an average value of 5.07%. It is demonstrated that the *fib* Model Code 2010 is the least accurate model in capturing the stress-strain behavior of SCC incorporating high-volume fly ash. The average value of COV computed by this model for the ascending part is 17.35%. However, it appears that all models give almost similar average values of COV when they are applied to capture the descending branch of the stress-strain diagram of SCC with high-volume fly ash. A higher value of COV in the descending branch indicates that the softening response of SCC with high-volume fly ash is more difficult to estimate. This phenomenon is also true for conventional concrete. It is known that the softening behavior is not solely material-dependent. Many factors affect the softening behavior, including the specimen or member geometry, the boundary conditions, the possibilities for load redistribution in the structure, the rigidity of the testing device, etc. [10,19].

4. CONCLUSIONS

The stress-strain behavior of SCC incorporating various high-volume levels of fly ash replacement was determined experimentally under uniaxial compression loading, where the deformation rate was controlled. Initially, the stress and strain showed a linear elastic relationship. The local and global longitudinal deformations were quite similar. At stress higher than 60% of the peak value, the local deformation tended to be greater than the global deformation, due to the localized fracture zone around the midheight of the specimen. The measurement of radial strain also confirmed the above situation. The values of ductility factors indicated that a higher fly ash content in the mix caused the SCC to be more ductile.

Several key parameters of stress-strain diagram were determined and used as inputs in the prediction of the complete stress-strain relationship using various models. It was concluded that the models were better at estimating the behavior of the ascending branch compared to the descending part. It was also shown that Samani and Attard's model gave better accuracy than the other models for predicting the complete stress-strain behavior of SCC incorporating high-volume fly ash.

5. ACKNOWLEDGEMENTS

This research was made possible due to financial support from the Universitas Sebelas Maret, through Mandatory Research Grant Contract No.623/UN27.21/PP/2017.

6. REFERENCES

[1] Mehta P. K., Conference Proceedings of the International Workshop on Sustainable Development and Concrete Technology, Edited by K Wang, Beijing, China, 2004, pp. 3-14

[2] Balakrishnan B., Awal A. S. M. A., Abdullah A. H. B., Hossain M. Z., Flow Properties and Strength Behaviour of Masonry Mortar Incorporating High Volume Fly Ash. International Journal of GEOMATE, Vol. 12, Issue No. 3 (SI. No. 31), 2017, pp. 121-126.

[3] Yoon S., Monteiro P. J. M., Macphee D. E., Glasser F. P., Statistical Evaluation of the Mechanical Properties of High-Volume Class F Fly Ash Concretes. Construction and Building Materials, Vol. 54, 2014, pp. 432-442.

[4] Sunarmasto., Kristiawan S. A., Effect of Fly Ash on Compressive Strength and Porosity of Self Compacting Concrete. Applied Mechanics and Materials, Vol. 754-755, 2015, pp. 447-451.

[5] Kristiawan S. A., Aditya M. T. M., Effect of High Volume Fly Ash on Shrinkage of Self-Compacting Concrete. Procedia Engineering, Vol. 125, 2015, pp. 705-712.

[6] Kristiawan S. A., Nugroho A. P., Creep Behaviour of Self-Compacting Concrete Incorporating High Volume Fly Ash and Its Effect on the Long-term Deflection of Reinforced Concrete Beam. Procedia Engineering, Vol. 171, 2017, pp. 715-724.

[7] Kristiawan S. A., Sunarmasto., Tyas G. P., Degradation of Self-Compacting Concrete (SCC) Due to Sulfuric Acid Attack: Experiment Investigation on the Effect of High Volume Fly Ash Content. IOP Conference Series: Materials Science and Engineering, Vol. 107, No 1, 2016, pp. 012029.

[8] Kristiawan S. A., Sunarmasto., Murti G. Y., Porosity of Self-Compacting Concrete (SCC) Incorporating High Volume Fly Ah. IOP Conference Series: Materials Science and Engineering, Vol. 176, No 1, 2016, pp. 012043.

[9] Kristiawan S., Wibowo., Sunarmasto., Gan B. S., Nurrohmah S., Estimating Corrosion Initiation Period Due to Chloride Ingress into Reinforced Self-Compacting Concrete Incorporating High Volume Fly Ash. Matec Web of Conferences, Vol. 102, 2017, pp. 01009

[10] International Federation for Structural Concrete *fib*., Model Code 2010, Vol. 1, 2012. pp. 127-129.

[11] International Federation for Structural Concrete *fib*., Constitutive Modelling of High Strength/High Performance Concrete, 2008.

[12] Jayaprithika S., Sekar S. K., Stress-strain Characteristics and Flexural Behaviour of Reinforced Eco-friendly Coconut Shell Concrete. Construction and Building Materials, Vol. 117, 2016, pp. 244-250.

[13] Belen G. F., Fernando M. A., Diego C. L. Sindy S. P., Stress-strain Relantionship in Axial Compression for Concrete Using Recycled Saturated Coarse Aggregate. Construction and Building Materials, Vol. 25, 2011, pp. 2335-2342.

[14] Da Y., Yu H., Ma H., Tan Y., Mi R., Dou X., Experimental Investigation of Whole Stress-strain Curves of Coral Concrete. Construction and Bilding Materials, Vol. 122, 2016, pp. 81-89.

[15] Noushini, A., Aslani F., Castel A., Gilbert G. I., Uy B., Compressive Stress-strain Model for Low-calcium Fly Ash-based Geopolymer and Heat-cured Portland Cement Concrete. Cement and Concrete Composites, Vol. 73, 2016, pp. 136-146.

[16] Okamura H., Ozawa K., Mix Design for Self-Compacting Concrete. Concrete Library of JSCE, Vol. 25, 1995, pp. 107-120.

[17] van Mier J. G. M., Failure of Concrete Under Uniaxial Compression: An Overview.

Fracture Mechanics of Concrete Structures, Proceeding FRAMCOS-3, AEDIFICATIO Publishers, Germany, pp. 1169-1181.

[18] Watanabe K., Niwa J., Yokota H., Iwanami M., Experimental Study on Stress-strain Curve of Concrete Considering Localized Failure in Compression. Journal of Advanced Concrete Technology, Vol. 2 No. 3, 2014, pp. 395-407.

[19] RILEM TC 148-SSC., Strain-softening of Concrete in Uniaxial Compression. Materials and Structures, Vol. 30, 1997, pp. 195-209.

[20] Carreira D., Chu K. H., Stress-strain Relationship for Plain Concrete in Ccompression. ACI Journal, Vol. Nov-Dec, 1985, pp. 797-804.

[21] Samani A. K., Attard M. M., A Stress-strain Model for Uniaxial and Confined Concrete Under Compression. Engineering Structures, Vol. 41, 2012, pp. 335-349.

[22] Guler K., Demir F., Pakdamar F., Stress-strain Modelling of High Srength Concrete by Fuzzy Logic Approach. Constructon and Building Materials, Vol. 37, 2012, pp. 680-684.

[23] Lim J. C., Ozbakkaloglu T., Stress-strain Model for Normal- and Light-weight Concretes Under Uniaxial and Triaxial Compression. Construction and Building Materials, Vol. 71, 2014, pp. 492-509.

[24] Wu J., Jing X., Wang Z., Uni-axial Compressive Stress-strain Relation of Recycled Coarse Aggregate Concrete After Freezing and Thwaing Cycle. Construction and Building Materials, Vol. 134, 2017, pp. 210-219.

[25] Nematzadeh M., Salari A., Ghadami J., Naghipour M., Stress-strain behaviour of Fresly Compressed Concrete Under Axial Compression with a Practical Equation. Construction and Building Materials, Vol. 115, 2016, pp. 402-423.

[26] Mohammadhosseini, H., Awal, A.S.M.A. and Ehsan, A.H., Influence of palm oil fuel ash on fresh and mechanical properties of self-compacting concrete, Sadhana-Academy Proceedings in Engineering Sciences, Vol.40, No.6, pp.1-11, 2015.

[27] Awal, A.S.M.A., Shehu, I.A. and Ismail, M., Effect of cooling regime on the residual